Temperature dependence of current-driven and Brownian skyrmion dynamics in ferrimagnets with compensation point

Markus Weißenhofer* and Ulrich Nowak
Fachbereich Physik, Universität Konstanz, DE-78457 Konstanz, Germany

(Received 19 December 2022; revised 2 February 2023; accepted 10 February 2023; published 24 February 2023)

Magnetic skyrmions are topological spin textures and promising candidates for novel spintronic applications. Recent studies on the current-driven dynamics of ferromagnetic (FM) skyrmions revealed that they exhibit an undesirable transverse motion, the skyrmion Hall effect. For antiferromagnetic (AFM) skyrmions, a vanishing skyrmion Hall effect was predicted, along with faster dynamics. However, their zero net magnetization obstructs efficient detection. Ferrimagnetic (FI) materials promise to combine both advantages: fast, AFM-like dynamics and easy read-out via stray fields. Here, we investigate the current-driven and Brownian dynamics of skyrmions in a FI with a compensation point. We perform atomistic spin dynamics simulations based on a model Hamiltonian and the stochastic Landau-Lifshitz-Gilbert equation supplemented with spin-orbit torques, accompanied by analytical calculations based on a collective coordinate approach. Our results unveil a nonmonotonic temperature dependence of the velocities and the diffusion coefficient with a strong enhancement at the angular momentum compensation temperature, due to scaling from FM- to AFM-like dynamics. These findings open up a new pathway for the efficient manipulation of skyrmion dynamics via temperature.

DOI: 10.1103/PhysRevB.107.064423

I. INTRODUCTION

Isolated magnetic skyrmions are topologically nontrivial, two-dimensional objects embedded in homogeneous magnetic phases [1,2]. They are characterized by a finite topological charge $Q = \frac{1}{4\pi}\int \boldsymbol{n}\cdot(\partial_x\boldsymbol{n}\times\partial_y\boldsymbol{n})\,d^2r$, indicating that the magnetic order parameter $\boldsymbol{n}$ spans the whole unit sphere, and are promising candidates as elements in future spintronic devices [3–5].

Ever since the first detection of magnetic skyrmions in MnSi in 2009 [6], most of the research focused on skyrmions in ferromagnetic (FM) materials, leading to the experimental demonstration of their current-driven [7–9] and Brownian motion [10–12] at room temperature in thin magnetic films. However, practical applicability of FM skyrmions is inevitably hindered by the skyrmion Hall effect [13,14], where the skyrmions acquire a finite velocity transverse to the current flow direction, due to a topology-dependent Magnus force [2].

To circumvent this problem, theoretical studies have suggested that the skyrmion Hall effect can be suppressed in antiferromagnetic (AFM) materials because the antiparallel orientation of the magnetization in the individual sublattices leads to opposing Magnus forces [15–17]. While the absence of a skyrmion Hall effect, together with the generally faster spin dynamics in AFMs [18], makes AFM skyrmions advantageous compared to their FM counterparts, their insensitivity to external magnetic fields obstructs efficient manipulation and detection.

Ferrimagnetic (FI) materials are composed of multiple antiferromagnetically coupled magnetic elements and offer the combined advantages of both FMs and AFMs, i.e., simple manipulation and detection using magnetic fields and fast AFM-like dynamics [19]. An exceptional representative of this class of magnetic materials are transition metal/rare earth compounds (e.g., Gd with Fe [20,21]), where the transition metal and rare earth moments are coupled antiferromagnetically and have different intrasublattice exchanges. As a result, the effective angular momentum of this type of FI gradually changes with temperature and disappears at a certain temperature below the Curie temperature, the so-called angular momentum compensation temperature. At this temperature, the dynamics of magnetic solitons become AFM-like, resulting in strongly enhanced domain wall motion [20–25] and a vanishing skyrmion Hall effect [26]. While they have been studied in multiple experiments [21,26–33], theoretical investigations of FI skyrmions are scarce at this point [34–36].

In this paper, we investigate the current-driven and Brownian motion of FI skyrmions using finite-temperature spin model calculations. We perform atomistic spin dynamics simulations based on the stochastic Landau-Lifshitz-Gilbert equation [37,38] supplemented with the SOTs [39] and a model Hamiltonian for a bilayer FI (see Fig. 1) with an angular momentum compensation point. Complementing the simulations, we calculate FI-skyrmion dynamics based on coupled Thiele equations [40] that we derive from a Lagrangian formulation of the multi-sublattice spin dynamics using a collective coordinate approach. Our results demonstrate a peak of the current-induced drift velocity, along with a sign switch of the SHA, and a strong enhancement of the Brownian motion at the angular momentum compensation temperature.

Our paper is organized as follows. In Sec. II, we present the derivation of the effective equation of motion for FI skyrmions, which is then subsequently used to derive

*markus.weissenhofer@uni-konstanz.de

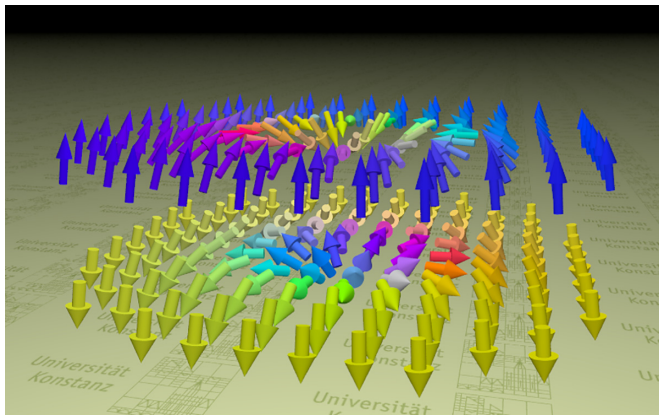

FIG. 1. The spin configuration of a skyrmion in a ferrimagnetic bilayer with the top and bottom layer constituting sublattice a and b, respectively. The colors indicate the direction of the spin vectors and the size indicates their angular momentum.

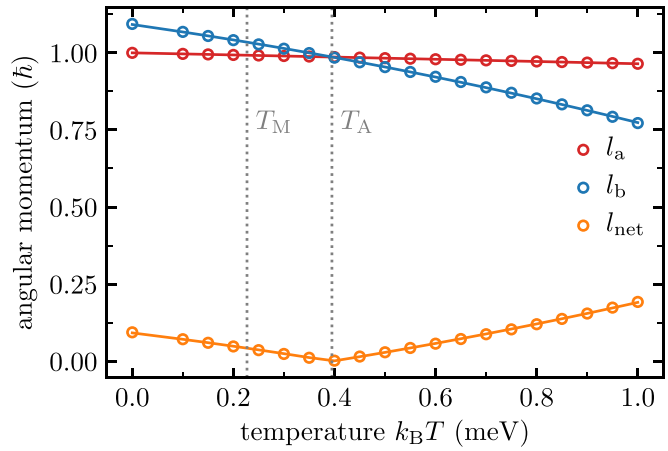

FIG. 2. Sublattice-specific and net thermal average angular momentum as a function of temperature (circles). Solid lines serve as guide to the eye. At the angular momentum compensation temperature T_A and the magnetization compensation temperature T_M, the net angular momentum and the net magnetization vanish, respectively. Note that $T_\mathrm{A} \neq T_\mathrm{M}$, due to our choice of $\gamma^\mathrm{a} \neq \gamma^\mathrm{b}$.

analytical formulas for the SOT-induced velocities and the diffusion coefficient. Section III summarizes the basics of atomistic spin models and the model parameters used within this study. Finally, in Sec. IV, we compare the results of our simulations with the theoretical formulas, followed by concluding remarks in Sec. V.

II. THEORY

A. Derivation of the equation of motion

Our starting point is a field theory description of the two-sublattice spin dynamics, where the spin configuration is assumed to be a continuous vector field. It can conveniently be expressed in terms of spherical coordinates via $\boldsymbol{S}_\nu = (\cos\Phi_\nu \sin\Theta_\nu, \sin\Phi_\nu \sin\Theta_\nu, \cos\Theta_\nu)$ with $\nu \in \{\mathrm{a}, \mathrm{b}\}$ and where $\Theta_\nu = \Theta_\nu(\boldsymbol{r}, t)$ and $\Phi_\nu = \Phi_\nu(\boldsymbol{r}, t)$ are continuous scalar functions.

The Lagrangian and the Rayleigh dissipation functional for the two-sublattice spin dynamics are given by

$$\mathcal{L} = -\frac{1}{a^2}\sum_\nu \int l_\nu \cos\Theta_\nu \dot{\Phi}_\nu \, d^2r - U, \tag{1}$$

$$\mathcal{R} = \frac{\alpha}{2a^2}\sum_\nu \int l_\nu \left(\dot{\Theta}_\nu^2 + \sin^2\Theta_\nu \dot{\Phi}_\nu^2\right) d^2r \tag{2}$$

with a being the lattice constant and $l_\nu = \mu_\nu/\gamma_\nu$ being the respective angular momenta of the two sublattices. Note that these angular momenta are temperature-dependent (see Fig. 2) since the effective magnetic moment is reduced by thermal fluctuations. U is the energy of the spin configuration that can be decomposed into three parts as $U = U_\mathrm{a} + U_\mathrm{b} + U_\mathrm{ab}$. The first two terms comprise the intrasublattice exchange. At this stage, their details are irrelevant, save for the fact that they allow for a stable skyrmion spin configuration. Instead we want to focus on the third term, U_ab, which describes the intersublattice exchange. The dominant contribution to this exchange stems from isotropic Heisenberg exchange. For sufficiently low spatial variation of the spin configuration and short-ranged interactions, we can assume that this energy can be well described by assuming local exchange between the two sublattices with $U_\mathrm{ab} = -J^\mathrm{ab}\frac{z}{a^2}\int \boldsymbol{S}_\mathrm{a}\cdot\boldsymbol{S}_\mathrm{b}\, d^2r$ and J^ab being the inter-sublattice exchange constant, see Sec. III, and z being the inter-sublattice coordination number.

As a next step, we employ a collective coordinate approach by assuming independent and rigid skyrmion motion [40] within each of the two sublattices. As such, the explicit time dependence of Θ_ν and Φ_ν is replaced by an implicit time dependence via $\Theta_\nu(\boldsymbol{r}, t) = \Theta_\nu(\boldsymbol{r} - \boldsymbol{R}_\nu(t))$ and $\Phi_\nu(\boldsymbol{r}, t) = \Phi_\nu(\boldsymbol{r} - \boldsymbol{R}_\nu(t))$, with $\boldsymbol{R}_\nu(t)$ being the position of the skyrmion within each sublattice. The temporal derivatives in Eqs. (1) and (2) thus become $\dot{\Theta}_\nu = -\boldsymbol{V}_\nu\cdot\nabla\Theta_\nu$ and $\dot{\Phi}_\nu = -\boldsymbol{V}_\nu\cdot\nabla\Phi_\nu$. Evaluating the corresponding Euler-Lagrange equations including dissipation for the dynamics of the skyrmion within each sublattice, $\partial_t(\partial\mathcal{L}/\partial\dot{\boldsymbol{R}}_\nu) - \partial\mathcal{L}/\partial\boldsymbol{R}_\nu + \partial\mathcal{R}/\partial\dot{\boldsymbol{R}}_\nu = 0$, yields two coupled Thiele equations [40] that read

$$\begin{aligned} l_\mathrm{a}(\boldsymbol{G}_\mathrm{a}\times\boldsymbol{V}_\mathrm{a} + \alpha\mathfrak{D}_\mathrm{a}\boldsymbol{V}_\mathrm{a}) &= -\frac{\partial(U_\mathrm{a}+U_\mathrm{ab})}{\partial\boldsymbol{R}_\mathrm{a}}, \\ l_\mathrm{b}(\boldsymbol{G}_\mathrm{b}\times\boldsymbol{V}_\mathrm{b} + \alpha\mathfrak{D}_\mathrm{b}\boldsymbol{V}_\mathrm{b}) &= -\frac{\partial(U_\mathrm{b}+U_\mathrm{ab})}{\partial\boldsymbol{R}_\mathrm{b}} \end{aligned} \tag{3}$$

with the gyrocoupling vector $\boldsymbol{G}_\nu = 4\pi Q_\nu \boldsymbol{e}_\perp/a^2$, where Q_ν are the respective topological charges of the skyrmions in each sublattice and $\boldsymbol{e}_\perp$ is a unit vector perpendicular to the film, and the trace of the dissipation tensor $\mathfrak{D}_\nu = \frac{1}{2a^2}\int(\partial_x\boldsymbol{S}_\nu)^2 + (\partial_y\boldsymbol{S}_\nu)^2\, d^2r$. Note that by using a scalar $\mathfrak{D}_\nu$, we implicitly assume cylindrical symmetry of the skyrmion spin configuration [41,42]. We have derived Eq. (3) under the assumption of rigid body motion. Hence, they do not include any mass terms that might stem from changes in shape or interactions with magnon modes. Mass terms, however, do not contribute to the steady state motion of magnetic textures driven by SOTs and to the diffusive motion, which are to be investigated here, and thus we neglect them in what follows. Since we also assume translational symmetry, the intrasublattice energies are independent of the skyrmion positions and therefore only

the intersublattice energy U_{ab} contributes to the forces on the right-hand side of Eq. (3).

Now we assume that the respective skyrmion spin configurations in the two sublattices can be transformed into each other by a simple translation and inversion of the spins, i.e., $\boldsymbol{S}_a(\boldsymbol{r}-\boldsymbol{R}_a) = -\boldsymbol{S}_b(\boldsymbol{r}-\boldsymbol{R}_b)$ for $\boldsymbol{R}_a = \boldsymbol{R}_b$. This is a convenient assumption for a rigid FI skyrmion and leads to $\boldsymbol{G}_\nu = \pm 4\pi \boldsymbol{e}_\perp/a^2$ and $\mathfrak{D}_a = \mathfrak{D}_b := \mathfrak{D}$. The intersublattice exchange becomes $U_{ab} = J^{ab}\frac{z}{a^2}\int \boldsymbol{S}(\boldsymbol{r}-\boldsymbol{R}_a)\cdot\boldsymbol{S}(\boldsymbol{r}-\boldsymbol{R}_b)\, d^2r$, which—up to second order for a cylindrically symmetric skyrmion—can be approximated as

$$U_{ab} \approx J^{ab}\frac{z}{a^2}\int \boldsymbol{S}^2(\boldsymbol{r})\, d^2r - \frac{J^{ab}z\mathfrak{D}}{2}(\boldsymbol{R}_a-\boldsymbol{R}_b)^2. \tag{4}$$

Note that we can neglect the subscript index of $\boldsymbol{S}(\boldsymbol{r})$ due to our aforementioned assumptions and that $J^{ab} < 0$ since we consider antiferromagnetic coupling between the two sublattices. The coupled Thiele equations (3) then transform to

$$\begin{aligned} l_a(\boldsymbol{G}\times\boldsymbol{V}_a + \alpha\mathfrak{D}\boldsymbol{V}_a) &= l_a\boldsymbol{F}_{ext} - \kappa(\boldsymbol{R}_a-\boldsymbol{R}_b),\\ l_b(-\boldsymbol{G}\times\boldsymbol{V}_b + \alpha\mathfrak{D}\boldsymbol{V}_b) &= l_b\boldsymbol{F}_{ext} + \kappa(\boldsymbol{R}_a-\boldsymbol{R}_b), \end{aligned} \tag{5}$$

where we introduced the abbreviation $\kappa = -J^{ab}z\mathfrak{D}$ and supplemented the right-hand side with an additional external force $l_\nu \boldsymbol{F}_{ext}$. Here we consider forces that stem from SOTs [43] and thermal fluctuations [44], both of which are proportional to the respective angular momenta and—apart from that—are equal on each sublattice. Henceforth, it is possible to write them as in (5).

As a last step, we introduce new variables, the FI skyrmion position $\boldsymbol{R}_{FI} = \frac{\boldsymbol{R}_a+\boldsymbol{R}_b}{2}$ and the internal displacement $\boldsymbol{d} = \boldsymbol{R}_a - \boldsymbol{R}_b$. Inversion of the matrices on the left-hand side of Eq. (5)—the crossproduct with the gyrocoupling vector can be expressed via a skew-symmetric matrix—and addition and subtraction of the equations yields

$$\dot{\boldsymbol{R}}_{FI} = \frac{1}{(\alpha\mathfrak{D})^2+G^2}\left[\frac{\Gamma+\Gamma^T}{2}\boldsymbol{F}_{ext} - \frac{\kappa}{2}\left(\frac{\Gamma}{l_a}-\frac{\Gamma^T}{l_b}\right)\boldsymbol{d}\right], \tag{6}$$

$$\dot{\boldsymbol{d}} = \frac{1}{(\alpha\mathfrak{D})^2+G^2}\left[(\Gamma-\Gamma^T)\boldsymbol{F}_{ext} - \kappa\left(\frac{\Gamma}{l_a}+\frac{\Gamma^T}{l_b}\right)\boldsymbol{d}\right], \tag{7}$$

where $\Gamma = \begin{pmatrix} \alpha\mathfrak{D} & G \\ -G & \alpha\mathfrak{D}\end{pmatrix}$. The second term in Eq. (6) gives rise to a coupling between the dynamics of $\boldsymbol{R}_{FI}$ and $\boldsymbol{d}$, which will be identified as being responsible for nonlinear dynamics and the compensation dependence of the gyrocoupling in the following two sections.

In a recent work [45], it was revealed that an additional contribution to the friction of a skyrmion emerges at finite temperatures due to the interaction with thermally excited magnons. The impact of this contribution is most pronounced at high temperatures and low values of the Gilbert damping. Here, however, we neglect this friction term in our analytical calculations (although this could be easily done by adding this term to the $\alpha\mathfrak{D}$ term). The reason for this is that for the parameters chosen here, the temperature dependence of the dynamics of FI skyrmions in the vicinity of the angular momentum compensation temperature is dominated by scaling of the effective gyrocoupling with the net angular momentum (see below), while the magnon-induced friction only has a minor impact.

B. Dynamics induced by a constant force

For constant external forces, the coupled first-order equations of motion for the position and angle of ferromagnetic domain walls can be transformed into a single equation describing only their position by eliminating the angular dynamics [46]. In doing so, the resulting equation of motion becomes a second-order differential equation due to the appearance of a Döring-mass term [47]. Hereinafter, we follow the calculations in Ref. [46] and derive a second-order equation of motion describing only the time evolution of the FI skyrmion position driven by a constant force (e.g., SOT-induced force) in a similar fashion.

First, we calculate the temporal derivative of Eq. (6) and substitute $\dot{\boldsymbol{d}}$ using Eq. (7). This yields

$$\begin{aligned} \ddot{\boldsymbol{R}}_{FI} = -\frac{\kappa}{2((\alpha\mathfrak{D})^2+G^2)^2}\left(\frac{\Gamma}{l_a}-\frac{\Gamma^T}{l_b}\right)\Bigg[(\Gamma-\Gamma^T)\boldsymbol{F}_{ext}\\ -\kappa\left(\frac{\Gamma}{l_a}+\frac{\Gamma^T}{l_b}\right)\boldsymbol{d}\Bigg]. \end{aligned} \tag{8}$$

Note that the first term in Eq. (6) drops out upon calculating the temporal derivative, since we assumed here that the force is constant and thus $\dot{\boldsymbol{F}}_{ext} = 0$. Now we again use Eq. (6) to express $\boldsymbol{d}$ in terms of $\dot{\boldsymbol{R}}_{FI}$ and $\boldsymbol{F}_{ext}$ and insert the resulting formula into Eq. (8). This yields

$$\frac{((\alpha\mathfrak{D})^2+G^2)l_al_b}{\kappa(l_a+l_b)}\dot{\boldsymbol{V}}_{FI} + \frac{l_a-l_b}{l_a+l_b}\boldsymbol{G}\times\boldsymbol{V}_{FI} + \alpha\mathfrak{D}\boldsymbol{V}_{FI} = \boldsymbol{F}_{ext}, \tag{9}$$

where $\boldsymbol{V}_{FI} = \dot{\boldsymbol{R}}_{FI}$. This equation describes the massive motion of a FI skyrmion induced by a constant force. The impact of the angular momenta l_a and l_b on the dynamics is twofold. First, they give rise to a mass term—a term that is proportional to $\ddot{\boldsymbol{R}}_{FI}$—where the prefactor can be interpreted as the effective mass of a FI skyrmion. The second effect is that the gyrocoupling term in Eq. (9) is weighted by the relative difference between the angular momenta of the two sublattices. As such, it manifests scaling between ferro- and antiferromagnetic behavior: if either l_a or l_b are zero (describing a single-sublattice FM), this factor reduces to ± 1, and—together with the fact that the mass-term vanishes—the above expression reduces to the usual Thiele equation describing the dynamics of ferromagnetic skyrmions [40]. For $l_a = l_b$ (describing an AFM), the gyrocoupling term vanishes, which is in line with what was reported for the dynamics of AFM skyrmions [15]. Note that the mass derived here differs from what was obtained in an earlier work based on a Lagrangian approach for the staggered magnetization in Ref. [34]. This is because the elimination of a degree of freedom, which is necessary to transform the first-order differential equations describing the dynamics to second-order differential equations, is done here on the level of the collective coordinates, whereas in Ref. [34] this was done on the level of Lagrangian description (by considering a massive Lagrangian for the staggered magnetization with a contribution $\mathcal{L}^{kin} \sim \int \dot{\boldsymbol{n}}^2\, d^2r$ [22]).

In the remainder of this section, however, we neglect the mass term. Instead, we focus on the steady-state motion of FI skyrmion driven by SOTs. The effective force acting on a skyrmion due to SOTs stems only from the damping-like torque (for details on the SOTs, see Sec. III) and is

given by $\boldsymbol{F}^{\mathrm{SOT}} = f^{\mathrm{SOT}}\boldsymbol{e}_\perp \times \boldsymbol{P}$ with $f^{\mathrm{SOT}} = \frac{\beta_d}{a^2}\int \partial_x[S_z]S_x - \partial_x[S_x]S_z\, d^2r$ [48]. Furthermore we assume that the effective spin polarization $\boldsymbol{P}$ is perpendicular to the current $\boldsymbol{j}$, i.e., $\boldsymbol{P} = \boldsymbol{e}_j \times \boldsymbol{e}_\perp$, as is done frequently in literature, see, e.g., Ref. [14]. For a current in x direction, the velocities then follow as

$$\boldsymbol{V}_{\mathrm{FI}} = \frac{f^{\mathrm{SOT}}}{(\alpha\mathfrak{D})^2 + G^2\left(\frac{l_\mathrm{a}-l_\mathrm{b}}{l_\mathrm{a}+l_\mathrm{b}}\right)^2}\begin{pmatrix}\alpha\mathfrak{D}\\ -G\frac{l_\mathrm{a}-l_\mathrm{b}}{l_\mathrm{a}+l_\mathrm{b}}\end{pmatrix}, \tag{10}$$

or, in terms of the absolute value of the velocity and the SHA,

$$|\boldsymbol{V}_{\mathrm{FI}}| = \frac{f^{\mathrm{SOT}}}{\sqrt{(\alpha\mathfrak{D})^2 + G^2\left(\frac{l_\mathrm{a}-l_\mathrm{b}}{l_\mathrm{a}+l_\mathrm{b}}\right)^2}}, \tag{11}$$

$$\Theta = -\tan^{-1}\left(\frac{G}{\alpha\mathfrak{D}}\frac{l_\mathrm{a}-l_\mathrm{b}}{l_\mathrm{a}+l_\mathrm{b}}\right). \tag{12}$$

From the above expressions, we expect a maximum of the absolute value of the velocity and a sign switch of the SHA at the angular momentum compensation temperature, i.e., if $l_\mathrm{a} = l_\mathrm{b}$, in line with what has been observed experimentally [26]. This is demonstrated using atomistic spin dynamics simulations below.

C. Calculating the diffusion coefficient

As laid out in Refs. [42,44,45,49,50] for FMs and in Ref. [15] for AFMs, Brownian motion of skyrmions can be described within the framework of the Thiele equation by substituting the external force with a stochastic force modeling thermal fluctuations. In an analogous manner, we replace $\boldsymbol{F}_{\mathrm{ext}}$ in Eq. (5), and consequently in Eqs. (6) and (7), with a stochastic force $\boldsymbol{F}^{\mathrm{th}}$ with the properties $\langle\boldsymbol{F}^{\mathrm{th}}\rangle = 0$ and $\langle\boldsymbol{F}^{\mathrm{th}}(t)(\boldsymbol{F}^{\mathrm{th}}(t'))^{\mathrm{T}}\rangle = 2k_\mathrm{B}T\alpha\mathfrak{D}\mathbb{1}\delta(t-t')$, in accordance with the fluctuation-dissipation theorem [51].

Equation (7) then becomes a first order linear stochastic differential equation,

$$\dot{\boldsymbol{d}}(t) = \underbrace{\frac{\Gamma-\Gamma^{\mathrm{T}}}{(\alpha\mathfrak{D})^2+G^2}}_{\omega}\boldsymbol{F}^{\mathrm{th}}(t) - \underbrace{\frac{\kappa}{(\alpha\mathfrak{D})^2+G^2}\left(\frac{\Gamma}{l_\mathrm{a}}+\frac{\Gamma^{\mathrm{T}}}{l_\mathrm{b}}\right)}_{\Omega}\boldsymbol{d}(t), \tag{13}$$

with the general solution [52]

$$\boldsymbol{d}(t) = e^{-\Omega t}\boldsymbol{d}(0) + \int_0^t e^{-\Omega(t-t')}\omega\boldsymbol{F}^{\mathrm{th}}(t')\,dt'. \tag{14}$$

Substitution of the solution in Eq. (6) yields

$$\dot{\boldsymbol{R}}_{\mathrm{FI}}(t) = \frac{1}{(\alpha\mathfrak{D})^2+G^2}\left[\frac{\Gamma+\Gamma^{\mathrm{T}}}{2}\boldsymbol{F}^{\mathrm{th}}(t) - \frac{\kappa}{2}\left(\frac{\Gamma}{l_\mathrm{a}}-\frac{\Gamma^{\mathrm{T}}}{l_\mathrm{b}}\right)\right.$$
$$\left.\times\left(e^{-\Omega t}\boldsymbol{d}(0) + \int_0^t e^{-\Omega(t-t')}\omega\boldsymbol{F}^{\mathrm{th}}(t')\,dt'\right)\right]. \tag{15}$$

The evaluation of the above expression requires the calculation of the matrix exponential $\exp(-\Omega t)$. This can be facilitated by using the decomposition $\Omega = \frac{\kappa}{c}(\alpha\mathfrak{D}g\mathbb{1} + Ghi\sigma_2)$ with $\sigma_2 = \left(\begin{smallmatrix}0 & -i\\ i & 0\end{smallmatrix}\right)$ being the second Pauli matrix and where we introduced the abbreviations $c = (\alpha\mathfrak{D})^2 + G^2$, $g = \frac{1}{l_\mathrm{a}} + \frac{1}{l_\mathrm{b}}$, and $h = \frac{1}{l_\mathrm{a}} - \frac{1}{l_\mathrm{b}}$. Now we use the Baker-Campbell-Hausdorff formula [53] and obtain $\exp(-\Omega t) = \exp(-\frac{\kappa}{c}\alpha\mathfrak{D}gt)\exp(-\frac{\kappa}{c}Ghi\sigma_2 t)$. The second exponential can be evaluated via its power series with $\sigma_2^2 = \mathbb{1}$, yielding $\exp(-\frac{\kappa}{c}Ghi\sigma_2 t) = \left(\begin{smallmatrix}\cos(\kappa Ght/c) & -\sin(\kappa Ght/c)\\ \sin(\kappa Ght/c) & \cos(\kappa Ght/c)\end{smallmatrix}\right) := \mathfrak{R}[\kappa Ght/c]$.

Inserting the evaluated matrix exponential into Eq. (15), assuming that $\boldsymbol{d}(0) = 0$ and temporal integration yields the displacement (details in Appendix),

$$\Delta\boldsymbol{R}_{\mathrm{FI}}(t) = \int_0^t \frac{\alpha\mathfrak{D}g^2\mathbb{1} - Gghi\sigma_2}{g^2(\alpha\mathfrak{D})^2 + G^2h^2}\boldsymbol{F}^{\mathrm{th}}(t')\,dt'$$
$$+\int_0^t \frac{\alpha\mathfrak{D}Ghi\sigma_2 - G^2g\mathbb{1}}{c(g^2(\alpha\mathfrak{D})^2 + G^2h^2)}e^{-\frac{\kappa}{c}\alpha\mathfrak{D}g(t-t')}$$
$$\times\left(Gh\mathfrak{R}\left[\frac{\kappa}{c}Ght(t-t') - \frac{\pi}{2}\right]\right.$$
$$\left.-\alpha\mathfrak{D}g\mathfrak{R}\left[\frac{\kappa}{c}Ght(t-t')\right]\right)\boldsymbol{F}^{\mathrm{th}}(t')\,dt'. \tag{16}$$

Only the first term contributes to the long-term behavior of the MSD $\langle\Delta\boldsymbol{R}_{\mathrm{FI}}(t)\Delta\boldsymbol{R}_{\mathrm{FI}}^{\mathrm{T}}(t)\rangle$. The diffusion tensor governs the long-term behavior of the MSD and can be calculated via $D^{\mathrm{tensor}} = \lim_{t\to\infty}\frac{\langle\Delta\boldsymbol{R}_{\mathrm{FI}}(t)\Delta\boldsymbol{R}_{\mathrm{FI}}^{\mathrm{T}}(t)\rangle}{2t}$. As demonstrated in Appendix, it is proportional to the unity matrix, i.e., $D^{\mathrm{tensor}} = D\mathbb{1}$, with D being the diffusion coefficient that can be calculated via

$$D = k_\mathrm{B}T\frac{\alpha\mathfrak{D}}{(\alpha\mathfrak{D})^2 + G^2\left(\frac{l_\mathrm{a}-l_\mathrm{b}}{l_\mathrm{a}+l_\mathrm{b}}\right)^2}. \tag{17}$$

Based on this formula, we expect a strong enhancement of the diffusion in the vicinity of the angular momentum compensation temperature, similar to the diffusion enhancement of skyrmions in synthetic antiferromagnets [54]. This is demonstrated using atomistic spin dynamics simulations below. Note that in the limits of $l_\mathrm{a} = l_\mathrm{b}$ or if either one of l_a or l_b are zero, Eq. (17) reduces to the respective formulas for the diffusion coefficients in AFMs [15] and FMs [49].

III. ATOMISTIC SPIN DYNAMICS SIMULATIONS

For our study, we model an ultrathin ferrimagnetic bilayer structure as shown in Fig. 1. Our atomistic spin model is based on the following spin Hamiltonian for the $2N$ normalized classical spins $\boldsymbol{S}_i^{\mathrm{a/b}}$ on a simple cubic lattice,

$$\mathcal{H} = -\sum_{i=1}^{N}\left[J^{\mathrm{ab}}\boldsymbol{S}_i^{\mathrm{a}}\cdot\boldsymbol{S}_i^{\mathrm{b}} + \frac{1}{2}\sum_{j=1}^{N}\left(J_{ij}^{\mathrm{aa}}\boldsymbol{S}_i^{\mathrm{a}}\cdot\boldsymbol{S}_j^{\mathrm{a}} + J_{ij}^{\mathrm{bb}}\boldsymbol{S}_i^{\mathrm{b}}\cdot\boldsymbol{S}_j^{\mathrm{b}}\right)\right]$$
$$-\frac{1}{2}\sum_{i=1}^{N}\sum_{j=1}^{N}\left(\boldsymbol{D}_{ij}^{\mathrm{aa}}\cdot\left(\boldsymbol{S}_i^{\mathrm{a}}\times\boldsymbol{S}_j^{\mathrm{a}}\right) + \boldsymbol{D}_{ij}^{\mathrm{bb}}\cdot\left(\boldsymbol{S}_i^{\mathrm{b}}\times\boldsymbol{S}_j^{\mathrm{b}}\right)\right)$$
$$-\sum_{i=1}^{N}\left(d^{\mathrm{a}}\left(S_i^{\mathrm{a},z}\right)^2 + d^{\mathrm{b}}\left(S_i^{\mathrm{b},z}\right)^2\right). \tag{18}$$

Both the intra- and intersublattice exchange are restricted to nearest neighbors. The Dzyaloshinsky-Moriya vectors [55,56] are assumed to be within the plane, i.e., $\boldsymbol{D}_{ij}^{\mathrm{aa/bb}} \perp \boldsymbol{r}_{ij}$ and $\boldsymbol{D}^{\mathrm{aa/bb}} \perp \boldsymbol{e}_z$, and the intersublattice Dzyaloshinsky-Moriya interaction is set to zero. The anisotropy constant $d^{\mathrm{a/b}} > 0$ define an easy axis in the direction perpendicular to the

film (here, the z axis). The parameters used throughout our study are given as follows: $J^{aa} = 10\,\text{meV}$, $J^{bb} = 0.1J^{aa}$, $J^{ab} = -0.1J^{aa}$, $D^{aa} = 0.3J^{aa}$, $D^{bb} = 0.03J^{aa}$, $d^{a} = 0.175J^{aa}$, and $d^{b} = 0.0175J^{aa}$. The parameters were chosen so that the skyrmion size is small and the diffusive motion is not too large, thus requiring only small system sizes and allowing for an efficient simulation, and that the drop of the net angular momentum at the angular momentum compensation temperature is rather steep, leading to pronounced peaks in the dynamics. Scaling the exchange parameters by a certain factor would simply result in the same scaling of the angular momentum compensation temperature. While the deterministic motion would be unaffected by this, since it only depends on the shape of the skyrmion (which would be unaltered), the diffusive motion would also increase by the same factor, requiring the simulation of larger systems.

The time evolution of the spins is calculated by means of the stochastic Landau-Lifshitz-Gilbert equation [37,38,57] supplemented with spin-orbit torques (SOTs)

$$\frac{\partial \boldsymbol{S}_i^\nu}{\partial t} = -\frac{\gamma^\nu}{(1+\alpha^2)\mu^\nu}\boldsymbol{S}_i^\nu \times \left(\boldsymbol{H}_i^\nu + \alpha \boldsymbol{S}_i^\nu \times \boldsymbol{H}_i^\nu\right) + \boldsymbol{T}_i^\nu \quad (19)$$

with $\nu \in \{a, b\}$, α being the Gilbert damping parameter and the effective field $\boldsymbol{H}_i^\nu = -\partial\mathcal{H}/\partial\boldsymbol{S}_i^\nu + \boldsymbol{\zeta}_i^\nu$. The latter contains both the deterministic field that stems from the spin Hamiltonian (18) and the stochastic field $\boldsymbol{\zeta}_i^\nu$ in the form of Gaussian white noise [58],

$$\left\langle \boldsymbol{\zeta}_i^\nu \right\rangle = 0 \quad \text{and} \quad \left\langle \boldsymbol{\zeta}_i^\nu(t)\left(\boldsymbol{\zeta}_j^\tau(0)\right)^{\mathrm{T}} \right\rangle = 2\frac{\alpha k_B T \mu^\nu}{\gamma^\nu}\delta_{\nu\tau}\delta_{ij}\delta(t)\mathbb{1}, \quad (20)$$

with k_B being the Boltzmann constant. For the atomic magnetic moments, we use $\mu^a = 2\,\mu_{\text{Bohr}}$ and $\mu^b = 2.1\,\mu_{\text{Bohr}}$. Using different gyromagnetic ratios of $\gamma^a = 2\,\mu_{\text{Bohr}}/\hbar = 1.76 \times 10^{11}\ \text{s}^{-1}\,\text{T}^{-1}$ and $\gamma^b = 0.96 \times 2\,\mu_{\text{Bohr}}/\hbar = 1.69 \times 10^{11}\ \text{s}^{-1}\,\text{T}^{-1}$ ensures that the magnetization compensation temperature and the angular momentum compensation temperature are different. For our chosen set of parameters we obtain a magnetization compensation temperature of $k_B T_M \approx 0.23\,\text{meV}$ and a angular momentum compensation temperature of $k_B T_A \approx 0.4\,\text{meV}$ ($T_A = 4.6\,\text{K}$), see Fig. 2.

In order to include the effect of spin-polarized currents on the FI skyrmions, the right-hand side of Eq. (19) is supplemented with the SOT terms [39]

$$\boldsymbol{T}_i^\nu = \frac{\beta_f - \alpha\beta_d}{1+\alpha^2}\boldsymbol{S}_i^\nu \times \boldsymbol{P} + \frac{\alpha\beta_f + \beta_d}{1+\alpha^2}\boldsymbol{S}_i^\nu \times \left(\boldsymbol{S}_i^\nu \times \boldsymbol{P}\right), \quad (21)$$

where $\boldsymbol{P}$ is the effective spin polarization direction and β_f and β_d are the strength of the fieldlike and dampinglike torque, respectively, that depend on the injected current density. Throughout our study we use $\beta_d = 1.25 \times 10^{10}\ \text{s}^{-1}$ and $\beta_f = 0$.

SOTs typically emerge due to a current in a heavy metal with high spin-orbit coupling adjacent to the magnetic layers [39]. As such, SOTs are an interface effect and their strength decays with the distance from the interface. Performing *ab initio* based calculations of the SOT profile is beyond the scope of this work and henceforth we make the ad-hoc assumption that the SOT acts equally on each sublattice. As such, our results can be directly transferred to skyrmions in a FI monolayer, where both sublattices are within the same layer. Note that analytical calculations similar to Sec. II for SOTs that act only on one of the layers suggest that there is no qualitative change to the dynamics. The only difference is that the external force in Eq. (9) is rescaled as $\boldsymbol{F}_{\text{ext}} \to \boldsymbol{F}_{\text{ext}} l_a/(l_a + l_b)$, for SOTs acting on layer a.

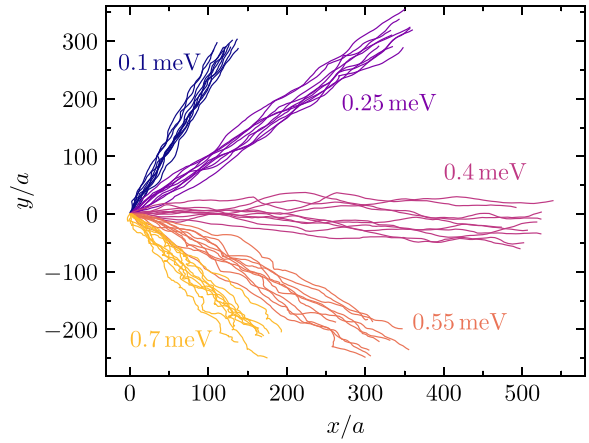

FIG. 3. Trajectories of FI skyrmions over 500 ps driven by spin-orbit torques with temperatures as labeled. The current is assumed to be in x direction and $\alpha = 0.01$.

The numerical integration of the stochastic Landau-Lifshitz-Gilbert equation with SOTs is performed via a GPU-based implementation of the Heun algorithm [57]. We simulate a system consisting of $64 \times 64 \times 2$ spins with a fixed timestep of 0.1 fs and with periodic boundary conditions in the in-plane directions. Initially, a FI skyrmion is placed in the center of the system and thermalized at finite temperature. Subsequently, its position is calculated every 0.1 ps over 0.5 ns from the spin configuration of sublattice a (since it less susceptible to thermal fluctuations, see Fig. 2) via $\boldsymbol{R}_{\text{FI}} = \sum_i \rho(\boldsymbol{S}_i^a)\boldsymbol{r}_i / \sum_i \rho(\boldsymbol{S}_i^a)$ with $\rho(\boldsymbol{S}_i^a) = (S_z^a - 0.4)^4 H(-S_z^a - 0.15)$, where $H(\dots)$ is the Heaviside function. This method has proven to be reliable both, for the thermal and the current-driven dynamics of skyrmions [41,42,45,49,54,59]. To provide sufficient statistics, we simulate the dynamics of 100 FI skyrmions for given values of the Gilbert damping and temperature, both for the Brownian and the SOT-induced motion.

IV. NUMERICAL RESULTS

A. Spin-orbit torque driven dynamics

Figure 3 shows five sets of trajectories obtained from simulations at temperatures as labeled. We find that the effect of finite temperatures is twofold. First, they lead to fluctuations of the trajectories, which are manifestations of Brownian motion superimposed on the deterministic SOT-induced drift motion. Second, they alter the drift motion itself: depending on temperature, the direction of motion of the FI skyrmions differ drastically. The SHA is found to be changing from positive to negative with increasing temperatures, together with a nonmonotonic behavior of the absolute value of the velocity.

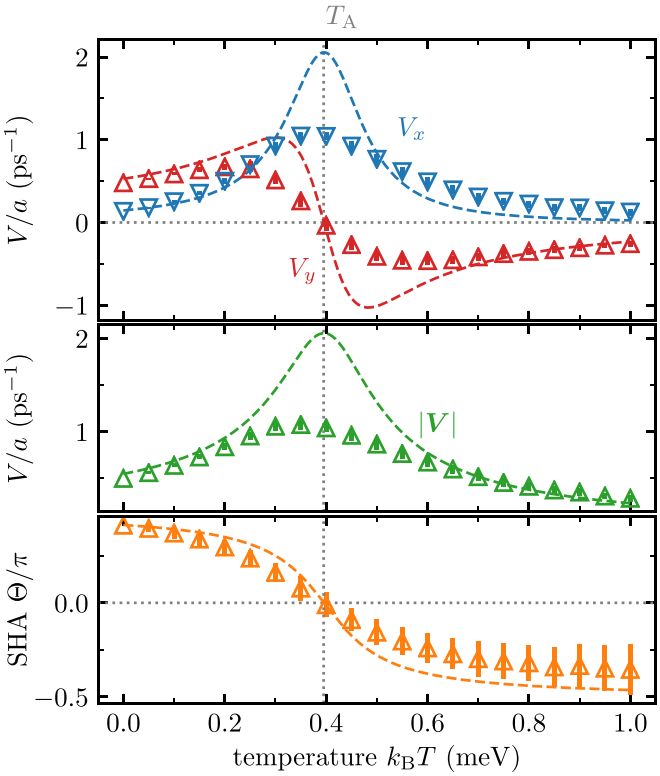

FIG. 4. Temperature dependence of SOT-induced velocities and the SHA of FI skyrmions for a current in x direction and with $\alpha = 0.01$. Dashed lines correspond to Eqs. (10)–(12) evaluated using the temperature-dependent angular momenta shown in Fig. 2.

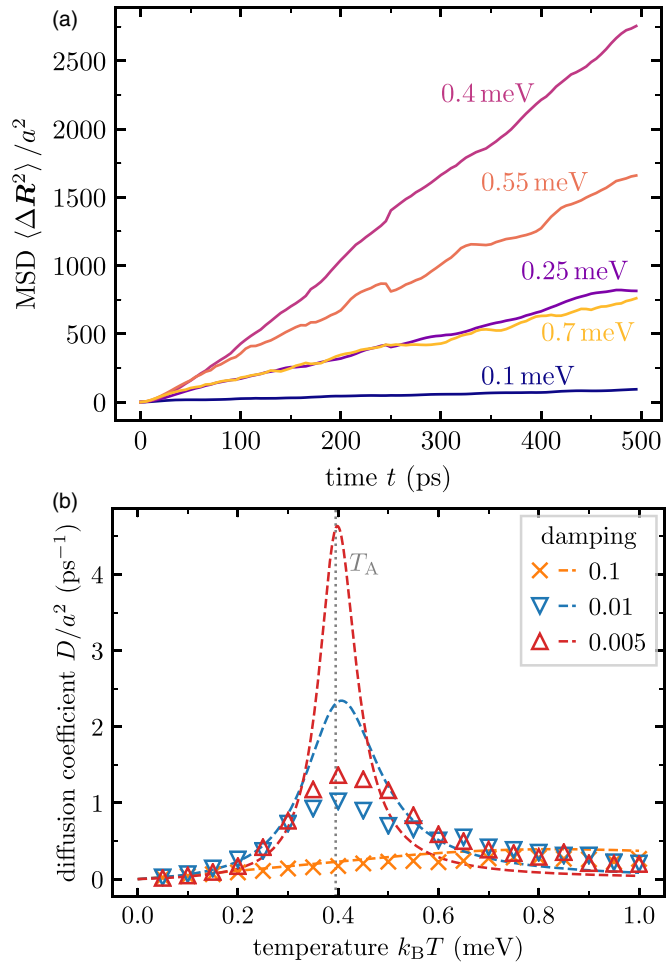

FIG. 5. Brownian motion of FI skyrmions. (a) MSD $\langle \Delta \boldsymbol{R}^2 \rangle$ with temperatures as labeled and with $\alpha = 0.005$. (b) Temperature dependence of diffusion coefficients obtained via a linear fit of $4Dt$ to the MSD $\langle \Delta \boldsymbol{R}^2 \rangle$ for different values of α. Dashed lines correspond to Eq. (17) evaluated using the temperature-dependent angular momenta shown in Fig. 2.

This is analyzed in more detail in Fig. 4, where the velocities and the SHA are shown for temperatures up to 1 meV. It can be observed that at the angular momentum compensation temperature T_A, the perpendicular velocity changes sign, resulting in sign change of the SHA, and the absolute value of the velocity as a maximum. This can be understood based on the fact that FI dynamics are AFM-like in the vicinity of T_A, which are characterized by a vanishing SHA and fast motion [15], and FM-like far away from T_A, with finite SHA. The dashed lines are the theoretical formulas derived in Sec. II B. We find that while in general the theory curves agree well with the simulation results, they tend to overestimate the peaks in the velocities. This can be related to the fact that we evaluate the theoretical predictions using the average of the angular momenta, whereas the effective angular momentum of a FI skyrmion undergoes thermal fluctuations. In the vicinity of a maximum of the velocity, these fluctuation of the effective angular momentum always lead to a reduction of the velocity. As such, this is a finite-size effect, because the fluctuations of the effective gyrocoupling go to zero for larger skyrmions. We have verified this assumption by varying the skyrmion size by changing the anisotropy constants (not shown here). Our results clearly demonstrate that for smaller anisotropy constants—and thus larger skyrmions—the ratio between the theoretical predictions and the simulation results becomes smaller.

In conclusion, albeit being AFM-like, the dynamics of FI skyrmions at the angular momentum compensation temperature are not as fast as the dynamics of AFM skyrmions, since the latter have proven to be in good quantitative agreement with analytical theory [15]. Based on this fact, we can also conclude that the difference in velocity between AFM skyrmions and FI skyrmions at the angular momentum compensation temperature is comparable to the difference between the theory curve and the simulations results for FI skyrmions at that temperature (cf. Fig. 4).

B. Brownian motion

Brownian motion is characterized by vanishing drift motion and a MSD that scales linearly with time. Typically, the MSD increases monotonously with temperature. This is, however, not the case for FI skyrmions, as is demonstrated in Fig. 5(a). We find that diffusive motion becomes maximal for $k_BT = 0.4$meV and that the MSDs for $k_BT = 0.25$meV and $k_BT = 0.7$meV are of similar magnitude.

A more detailed analysis of this behavior can be found in Fig. 5(b), where the diffusion coefficients are shown for different values of the Gilbert damping parameter and for

different temperatures. Again, the dashed lines correspond to theoretical formula derived in Sec. II B. For $\alpha = 0.01$ and 0.005, we find a pronounced peak of the diffusion coefficient at the angular momentum compensation temperature. The reason for this is that the dynamics of a FI skyrmions are AFM-like in the vicinity of T_A, which is associated with high skyrmion diffusion [15] for low Gilbert damping, and FM-like far away from T_A, where skyrmion diffusion is suppressed by the gyrocoupling [49]. Note that we do not find a peak of the diffusion coefficient for $\alpha = 0.1$, in line with the theoretical prediction. This is because for this value of the Gilbert damping, the difference between FM- and AFM-like skyrmion diffusion is less pronounced.

Similar to the SOT-driven motion, we find that our theory based on the collective coordinate approach provides reasonable agreement with the simulation results, although the peaks are greatly overestimated by it. Again, this can be related to the fluctuation of the effective angular momentum of the FI skyrmion, giving rise to reduced diffusion of FI skyrmions as compared to their AFM counterpart [15], even in the vicinity of T_A.

V. CONCLUSION

In conclusion, we have studied the current-driven and Brownian motion of FI skyrmions using both, atomistic spin dynamics simulations based on the stochastic Landau-Lifshitz-Gilbert equation and analytical calculations based on a collective coordinate approach. Our results clearly demonstrate a nonmonotonic temperature dependence of the SOT-induced velocities and the diffusion coefficients with a pronounced peak at the angular momentum compensation temperature, rather than the magnetization compensation temperature. This behavior can be explained by scaling of the effective gyrocoupling of FI skyrmions with the temperature-dependent net angular momentum of the system. In addition, our results reveal that thermal fluctuations of the net angular momentum lead to a reduction of the peaks in the velocities and the diffusion coefficient, giving rise to slower dynamics of FI skyrmions as compared to AFM skyrmions even at the angular momentum compensation temperature.

The nonmonotonic temperature dependence of the dynamics of FI skyrmions distinguishes them from their FM and AFM counterparts. It can be exploited for efficient manipulation of their current-driven and Brownian motion by temperature, which could be of advantage in future spintronic devices.

ACKNOWLEDGMENTS

The authors thank Levente Rózsa and Severin Selzer for fruitful discussions. This work was financially supported by the Deutsche Forschungsgemeinschaft (DFG, German Research Foundation) through Project No. 403502522 and the SFB 1432.

APPENDIX: DERIVATION OF DIFFUSION COEFFICIENT FORMULA

In this section, we present in detail the derivation of the diffusion coefficient for a FI skyrmion. We start with the coupled first-order linear stochastic differential equations that we obtain by supplementing Eqs. (6) and (7) with a stochastic force,

$$\begin{aligned}\dot{\boldsymbol{R}}_{\mathrm{FI}}(t) &= \frac{\Gamma+\Gamma^{\mathrm{T}}}{2c}\boldsymbol{F}^{\mathrm{th}}(t) - \frac{\kappa}{2c}\left(\frac{\Gamma}{l_{\mathrm{a}}} - \frac{\Gamma^{\mathrm{T}}}{l_{\mathrm{b}}}\right)\boldsymbol{d}(t),\\ \dot{\boldsymbol{d}}(t) &= \underbrace{\frac{\Gamma-\Gamma^{\mathrm{T}}}{c}}_{\omega}\boldsymbol{F}^{\mathrm{th}}(t) - \underbrace{\frac{\kappa}{c}\left(\frac{\Gamma}{l_{\mathrm{a}}} + \frac{\Gamma^{\mathrm{T}}}{l_{\mathrm{b}}}\right)}_{\Omega}\boldsymbol{d}(t)\end{aligned}, \tag{A1}$$

where $c = (\alpha\mathfrak{D})^2 + G^2$, $\langle \boldsymbol{F}^{\mathrm{th}}\rangle = 0$ and $\langle \boldsymbol{F}^{\mathrm{th}}(t)(\boldsymbol{F}^{\mathrm{th}}(t'))^{\mathrm{T}}\rangle = 2\alpha\mathfrak{D}k_{\mathrm{B}}T\mathbb{1}\delta(t-t')$. Being independent of $\boldsymbol{R}_{\mathrm{FI}}$, the equation for $\boldsymbol{d}$ can be solved individually and has the general solution [52]

$$\boldsymbol{d}(t) = e^{-\Omega t}\boldsymbol{d}(0) + \int_0^t e^{-\Omega(t-t')}\omega\boldsymbol{F}^{\mathrm{th}}(t')\,dt'. \tag{A2}$$

Insertion of the solution into the equation for $\dot{\boldsymbol{R}}_{\mathrm{FI}}$ yields

$$\begin{aligned}\dot{\boldsymbol{R}}_{\mathrm{FI}}(t) = \frac{\Gamma+\Gamma^{\mathrm{T}}}{2c}\boldsymbol{F}^{\mathrm{th}}(t) - \frac{\kappa}{2c}\left(\frac{\Gamma}{l_{\mathrm{a}}} - \frac{\Gamma^{\mathrm{T}}}{l_{\mathrm{b}}}\right)\\ \times\left(e^{-\Omega t}\boldsymbol{d}(0) + \int_0^t e^{-\Omega(t-t')}\omega\boldsymbol{F}^{\mathrm{th}}(t')\,dt'\right).\end{aligned} \tag{A3}$$

As argued in Sec. II, the matrix exponential $e^{-\Omega t}$ can be evaluated as

$$e^{-\Omega t} = e^{-\frac{\kappa}{c}\alpha\mathfrak{D}gt}\underbrace{\begin{pmatrix}\cos(\kappa Ght/c) & -\sin(\kappa Ght/c)\\ \sin(\kappa Ght/c) & \cos(\kappa Ght/c)\end{pmatrix}}_{\mathfrak{R}[\kappa Ght/c]} \tag{A4}$$

with $\sigma_2 = \left(\begin{smallmatrix}0 & -i\\ i & 0\end{smallmatrix}\right)$ being the second Pauli matrix and where we introduced the abbreviations $g = \frac{1}{l_{\mathrm{a}}} + \frac{1}{l_{\mathrm{b}}}$ and $h = \frac{1}{l_{\mathrm{a}}} - \frac{1}{l_{\mathrm{b}}}$. As a next step, we assume that $\boldsymbol{d}(0) = 0$ and calculate the displacement $\Delta\boldsymbol{R}(t) = \int_0^t dt'\,\dot{\boldsymbol{R}}_{\mathrm{FI}}(t')$ via

$$\Delta\boldsymbol{R}_{\mathrm{FI}}(t) = \int_0^t \frac{\alpha\mathfrak{D}}{c}\boldsymbol{F}^{\mathrm{th}}(t')\,dt' - \frac{G\kappa}{c^2}(\alpha\mathfrak{D}h\mathbb{1} + Gi\sigma_2)\int_0^t\int_0^{t'} e^{-\frac{\kappa}{c}\alpha\mathfrak{D}g(t'-t'')}\mathfrak{R}\left[\frac{\kappa}{c}Gh(t'-t'')\right]i\sigma_2\boldsymbol{F}^{\mathrm{th}}(t'')\,dt''dt' \tag{A5}$$

$$= \int_0^t \frac{\alpha\mathfrak{D}}{c}\boldsymbol{F}^{\mathrm{th}}(t')\,dt' - \frac{G\kappa}{c^2}(\alpha\mathfrak{D}h\mathbb{1} + Gi\sigma_2)\int_0^t\int_{t''}^t e^{-\frac{\kappa}{c}\alpha\mathfrak{D}g(t'-t'')}\mathfrak{R}\left[\frac{\kappa}{c}Gh(t'-t'')\right]i\sigma_2\boldsymbol{F}^{\mathrm{th}}(t'')\,dt'dt'' \tag{A6}$$

$$= \int_0^t dt' \, \frac{\alpha\mathfrak{D}}{c} \boldsymbol{F}^{\mathrm{th}}(t') - \frac{G}{c} \frac{\alpha\mathfrak{D}h\mathbb{1} + Gg i\sigma_2}{g^2(\alpha\mathfrak{D})^2 + G^2h^2} \int_0^t \Bigg[\alpha\mathfrak{D}g\mathbb{1} - Ghi\sigma_2$$

$$+ e^{-\frac{\kappa}{c}\alpha\mathfrak{D}g(t-t'')} \left(Gh\Re\left[\frac{\kappa}{c}Gh(t-t'') - \pi/2\right] - \alpha\mathfrak{D}g\Re\left[\frac{\kappa}{c}Gh(t-t'')\right]\right)\Bigg] i\sigma_2 \boldsymbol{F}^{\mathrm{th}}(t'')\, dt'' \tag{A7}$$

$$= \frac{\alpha\mathfrak{D}g^2\mathbb{1} - Gghi\sigma_2}{g^2(\alpha\mathfrak{D})^2 + G^2h^2} \int_0^t \boldsymbol{F}^{\mathrm{th}}(t')\, dt' - \frac{G}{c} \frac{\alpha\mathfrak{D}h\mathbb{1} + Gg i\sigma_2}{g^2(\alpha\mathfrak{D})^2 + G^2h^2} \int_0^t e^{-\frac{\kappa}{c}\alpha\mathfrak{D}g(t-t')}$$

$$\times \left(Gh\Re\left[\frac{\kappa}{c}Gh(t-t') - \pi/2\right] - \alpha\mathfrak{D}g\Re\left[\frac{\kappa}{c}Gh(t-t')\right]\right) i\sigma_2 \boldsymbol{F}^{\mathrm{th}}(t')\, dt', \tag{A8}$$

where in the first step, we changed the order of the integration over dt' and dt'' and in the second step we performed the integration over dt', using the fact that $\Re[\dots]$ consists of sine and cosine functions.

The long-term behavior of the MSD is governed by the first term in the above expression, whereas the second term only contributes to the short-term dynamics. The diffusion tensor thus follows as

$$D^{\mathrm{tensor}} = \lim_{t\to\infty} \frac{\left\langle \Delta\boldsymbol{R}_{\mathrm{FI}}(t) \Delta\boldsymbol{R}_{\mathrm{FI}}^{\mathrm{T}}(t)\right\rangle}{2t} \tag{A9}$$

$$= \lim_{t\to\infty} \frac{1}{2t} \left\langle \int_0^t \left[\frac{\alpha\mathfrak{D}g^2\mathbb{1} - Gghi\sigma_2}{g^2(\alpha\mathfrak{D})^2 + G^2h^2}\right] \boldsymbol{F}^{\mathrm{th}}(t')\, dt' \int_0^t (\boldsymbol{F}^{\mathrm{th}}(t''))^{\mathrm{T}} \left[\frac{\alpha\mathfrak{D}g^2\mathbb{1} + Gghi\sigma_2}{g^2(\alpha\mathfrak{D})^2 + G^2h^2}\right] dt'' \right\rangle \tag{A10}$$

$$= \frac{\lim_{t\to\infty} \frac{1}{2t} \int_0^t \int_0^t 2\alpha\mathfrak{D}k_{\mathrm{B}}T\mathbb{1}\delta(t'-t'')\, dt' dt''}{(\alpha\mathfrak{D})^2 + G^2\frac{h^2}{g^2}} \tag{A11}$$

$$= k_{\mathrm{B}}T \frac{\alpha\mathfrak{D}}{(\alpha\mathfrak{D})^2 + G^2\frac{h^2}{g^2}}\mathbb{1}. \tag{A12}$$

The diffusion tensor is proportional to the unity matrix, indicating that Brownian motion is isotropic. We define the diffusion coefficient as the prefactor before the unity matrix that, recalling the definitions of g and h, is finally obtained as

$$D = k_{\mathrm{B}}T \frac{\alpha\mathfrak{D}}{(\alpha\mathfrak{D})^2 + G^2\left(\frac{l_{\mathrm{a}}-l_{\mathrm{b}}}{l_{\mathrm{a}}+l_{\mathrm{b}}}\right)^2}. \tag{A13}$$

In the limits of $l_{\mathrm{a}} = l_{\mathrm{b}}$ or if either one of l_{a} or l_{b} are zero, the above expression reduces to the respective formulas for the diffusion coefficients in AFM [15] and FM systems [49]. We note that one would also get this expression by replacing the constant force in Eq. (9) with the fluctuating force $\boldsymbol{F}^{\mathrm{th}}$. However, this is not justified since Eq. (9) was derived specifically under the assumption that the force is constant. Moreover, the short-term behavior predicted by Eq. (9) supplemented with a fluctuating force is different from what one would obtain from solving the coupled stochastic differential equations in $\boldsymbol{R}_{\mathrm{FI}}$ and $\boldsymbol{d}$.

[1] A. Bogdanov and A. Hubert, J. Magn. Magn. Mater. **138**, 255 (1994).

[2] N. Nagaosa and Y. Tokura, Nat. Nanotechnol. **8**, 899 (2013).

[3] A. Fert, V. Cros, and J. Sampaio, Nat. Nanotechnol. **8**, 152 (2013).

[4] D. Pinna, F. Abreu Araujo, J.-V. Kim, V. Cros, D. Querlioz, P. Bessiere, J. Droulez, and J. Grollier, Phys. Rev. Appl. **9**, 064018 (2018).

[5] Y. Jibiki, M. Goto, E. Tamura, J. Cho, S. Miki, R. Ishikawa, H. Nomura, T. Srivastava, W. Lim, S. Auffret, C. Baraduc, H. Bea, and Y. Suzuki, Appl. Phys. Lett. **117**, 082402 (2020).

[6] S. Mühlbauer, B. Binz, F. Jonietz, C. Pfleiderer, A. Rosch, A. Neubauer, R. Georgii, and P. Böni, Science **323**, 915 (2009).

[7] W. Jiang, P. Upadhyaya, W. Zhang, G. Yu, M. B. Jungfleisch, F. Y. Fradin, J. E. Pearson, Y. Tserkovnyak, K. L. Wang, O. Heinonen, S. G. E. te Velthuis, and A. Hoffmann, Science **349**, 283 (2015).

[8] S. Woo, K. Litzius, B. Krüger, M.-Y. Im, L. Caretta, K. Richter, M. Mann, A. Krone, R. M. Reeve, M. Weigand, P. Agrawal, I. Lemesh, M.-A. Mawass, P. Fischer, M. Kläui, and G. S. D. Beach, Nat. Mater. **15**, 501 (2016).

[9] W. Legrand, D. Maccariello, N. Reyren, K. Garcia, C. Moutafis, C. Moreau-Luchaire, S. Collin, K. Bouzehouane, V. Cros, and A. Fert, Nano Lett. **17**, 2703 (2017).

[10] J. Zázvorka, F. Jakobs, D. Heinze, N. Keil, S. Kromin, S. Jaiswal, K. Litzius, G. Jakob, P. Virnau, D. Pinna, K. Everschor-Sitte, L. Rózsa, A. Donges, U. Nowak, and M. Kläui, Nat. Nanotechnol. **14**, 658 (2019).

[11] T. Nozaki, Y. Jibiki, M. Goto, E. Tamura, T. Nozaki, H. Kubota, A. Fukushima, S. Yuasa, and Y. Suzuki, Appl. Phys. Lett. **114**, 012402 (2019).

[12] L. Zhao, Z. Wang, X. Zhang, X. Liang, J. Xia, K. Wu, H.-A. Zhou, Y. Dong, G. Yu, K. L. Wang, X. Liu, Y. Zhou, and W. Jiang, Phys. Rev. Lett. **125**, 027206 (2020).

[13] W. Jiang, X. Zhang, G. Yu, W. Zhang, X. Wang, M. Jungfleisch, J. Pearson, X. Cheng, O. Heinonen, K. L. Wang, Y. Zhou, A. Hoffmann, and S. G. E. te Velthuis, Nat. Phys. **13**, 162 (2017).

[14] K. Litzius, I. Lemesh, B. Krüger, P. Bassirian, L. Caretta, K. Richter, F. Büttner, K. Sato, O. A. Tretiakov, J. Förster, R. M. Reeve, M. Weigand, I. Bykova, H. Stoll, G. Schütz, G. S. D. Beach, and M. Kläui, Nat. Phys. **13**, 170 (2017).

[15] J. Barker and O. A. Tretiakov, Phys. Rev. Lett. **116**, 147203 (2016).

[16] X. Zhang, Y. Zhou, and M. Ezawa, Nat. Commun. **7**, 10293 (2016).

[17] C. Jin, C. Song, J. Wang, and Q. Liu, Appl. Phys. Lett. **109**, 182404 (2016).

[18] T. Jungwirth, X. Marti, P. Wadley, and J. Wunderlich, Nat. Nanotechnol. **11**, 231 (2016).

[19] S. K. Kim, G. S. D. Beach, K.-J. Lee, T. Ono, T. Rasing, and H. Yang, Nat. Mater. **21**, 24 (2022).

[20] K.-J. Kim, S. K. Kim, Y. Hirata, S.-H. Oh, T. Tono, D.-H. Kim, T. Okuno, W. S. Ham, S. Kim, G. Go, Y. Tserkovnyak, A. Tsukamoto, T. Moriyama, K.-J. Lee, and T. Ono, Nat. Mater. **16**, 1187 (2017).

[21] L. Caretta, M. Mann, F. Büttner, K. Ueda, B. Pfau, C. M. Günther, P. Hessing, A. Churikova, C. Klose, M. Schneider, D. Engel, C. Marcus, D. Bono, K. Bagschik, S. Eisebitt, and G. S. D. Beach, Nat. Nanotechnol. **13**, 1154 (2018).

[22] E. V. Gomonay and V. M. Loktev, Low Temp. Phys. **40**, 17 (2014).

[23] S. Selzer, U. Atxitia, U. Ritzmann, D. Hinzke, and U. Nowak, Phys. Rev. Lett. **117**, 107201 (2016).

[24] S. A. Siddiqui, J. Han, J. T. Finley, C. A. Ross, and L. Liu, Phys. Rev. Lett. **121**, 057701 (2018).

[25] A. Donges, N. Grimm, F. Jakobs, S. Selzer, U. Ritzmann, U. Atxitia, and U. Nowak, Phys. Rev. Res. **2**, 013293 (2020).

[26] Y. Hirata, D.-H. Kim, S. K. Kim, D.-K. Lee, S.-H. Oh, D.-Y. Kim, T. Nishimura, T. Okuno, Y. Futakawa, H. Yoshikawa, A. Tsukamoto, Y. Tserkovnyak, Y. Shiota, T. Moriyama, S.-B. Choe, K.-J. Lee, and T. Ono, Nat. Nanotechnol. **14**, 232 (2019).

[27] S. Woo, K. M. Song, X. Zhang, Y. Zhou, M. Ezawa, X. Liu, S. Finizio, J. Raabe, N. J. Lee, S.-I. Kim, S.-Y. Park, Y. Kim, J.-Y. Kim, D. Lee, O. Lee, J. W. Choi, B.-C. Min, H. C. Koo, and J. Chang, Nat. Commun. **9**, 959 (2018).

[28] J. Brandão, D. A. Dugato, M. V. Puydinger dos Santos, and J. C. Cezar, ACS Appl. Nano Mater. **2**, 7532 (2019).

[29] S. Ding, A. Ross, R. Lebrun, S. Becker, K. Lee, I. Boventer, S. Das, Y. Kurokawa, S. Gupta, J. Yang, G. Jakob, and M. Kläui, Phys. Rev. B **100**, 100406(R) (2019).

[30] K. Chen, D. Lott, A. Philippi-Kobs, M. Weigand, C. Luo, and F. Radu, Nanoscale **12**, 18137 (2020).

[31] H. Wu, F. Groß, B. Dai, D. Lujan, S. A. Razavi, P. Zhang, Y. Liu, K. Sobotkiewich, J. Förster, M. Weigand, G. Schütz, X. Li, J. Gräfe, and K. L. Wang, Adv. Mater. **32**, 2003380 (2020).

[32] C. T. Ma, T. Q. Hartnett, W. Zhou, P. V. Balachandran, and S. J. Poon, Appl. Phys. Lett. **119**, 192406 (2021).

[33] S. Vélez, S. Ruiz-Gómez, J. Schaab, E. Gradauskaite, M. S. Wörnle, P. Welter, B. J. Jacot, C. L. Degen, M. Trassin, M. Fiebig, and P. Gambardella, Nat. Nanotechnol. **17**, 834 (2022).

[34] S. K. Kim, K.-J. Lee, and Y. Tserkovnyak, Phys. Rev. B **95**, 140404(R) (2017).

[35] C. T. Ma, Y. Xie, H. Sheng, A. W. Ghosh, and S. J. Poon, Sci. Rep. **9**, 9964 (2019).

[36] S. K. Kim, K. Nakata, D. Loss, and Y. Tserkovnyak, Phys. Rev. Lett. **122**, 057204 (2019).

[37] L. D. Landau and E. M. Lifshitz, Phys. Z. Sowjetunion **8**, 101 (1935); reprinted in Ukr. J. Phys. **53**, Special Issue, 14 (2008).

[38] T. L. Gilbert, IEEE Trans. Magn. **40**, 3443 (2004).

[39] A. Manchon, J. Železný, I. M. Miron, T. Jungwirth, J. Sinova, A. Thiaville, K. Garello, and P. Gambardella, Rev. Mod. Phys. **91**, 035004 (2019).

[40] A. A. Thiele, Phys. Rev. Lett. **30**, 230 (1973).

[41] M. Weißenhofer and U. Nowak, Phys. Rev. B **99**, 224430 (2019).

[42] M. Weißenhofer and U. Nowak, New J. Phys. **22**, 103059 (2020).

[43] U. Ritzmann, S. von Malottki, J.-V. Kim, S. Heinze, J. Sinova, and B. Dupé, Nature Electronics **1**, 451 (2018).

[44] R. E. Troncoso and Á. S. Núñez, Ann. Phys. **351**, 850 (2014).

[45] M. Weißenhofer, L. Rózsa, and U. Nowak, Phys. Rev. Lett. **127**, 047203 (2021).

[46] A. Malozemoff and J. Slonczewski, *Magnetic Domain Walls in Bubble Materials*, edited by A. Malozemoff and J. Slonczewski (Academic Press, New York, 1979), pp. 123-143.

[47] W. Döring, Z. Naturforschung A **3**, 373 (1948).

[48] J. Sampaio, V. Cros, S. Rohart, A. Thiaville, and A. Fert, Nat. Nanotechnol. **8**, 839 (2013).

[49] C. Schütte, J. Iwasaki, A. Rosch, and N. Nagaosa, Phys. Rev. B **90**, 174434 (2014).

[50] J. Miltat, S. Rohart, and A. Thiaville, Phys. Rev. B **97**, 214426 (2018).

[51] R. Kubo, Rep. Prog. Phys. **29**, 255 (1966).

[52] B. Øksendal, *Stochastic Differential Equations An Introduction with Applications*, Vol. 82 (Springer, Berlin, Heidelberg, 2000).

[53] B. C. Hall, *Lie Groups, Lie Algebras, and Representations An Elementary Introduction* (Springer, Cham, 2003).

[54] T. Dohi, M. Weißenhofer, N. Kerber, F. Kammerbauer, Y. Ge, K. Raab, J. ZÃ zvorka, M.-A. Syskaki, A. Shahee, M. Ruhwedel, T. Böttcher, P. Pirro, G. Jakob, U. Nowak, and M. Kläui, Enhanced thermally-activated skyrmion diffusion in synthetic antiferromagnetic systems with tunable effective topological charge, arXiv:2206.00791.

[55] I. Dzyaloshinskii, J. Phys. Chem. Solids **4**, 241 (1958).

[56] T. Moriya, Phys. Rev. **120**, 91 (1960).

[57] U. Nowak, Classical spin models, *Handbook of Magnetism and Advanced Magnetic Materials*, edited by H. Kronmüller and S. Parkin (Wiley, New York, 2007).

[58] W. F. Brown, Phys. Rev. **130**, 1677 (1963).

[59] M. Weißenhofer and U. Nowak, Sci. Rep. **12**, 6801 (2022).